

Test of Pseudospin Symmetry in Deformed Nuclei

J.N. Ginocchio,^{1,*} A. Leviatan,^{2,†} J. Meng,^{3,‡} and Shan-Gui Zhou^{4,3,§}

¹*Theoretical Division, Los Alamos National Laboratory, Los Alamos, New Mexico 87545, USA*

²*Racah Institute of Physics, The Hebrew University, Jerusalem 91904, Israel*

³*School of Physics, Peking University, Beijing 100871, China*

⁴*Max-Planck Institute for Nuclear Physics, 69029 Heidelberg, Germany*

(Dated: March 30, 2022)

Pseudospin symmetry is a relativistic symmetry of the Dirac Hamiltonian with scalar and vector mean fields equal and opposite in sign. This symmetry imposes constraints on the Dirac eigenfunctions. We examine extensively the Dirac eigenfunctions of realistic relativistic mean field calculations of deformed nuclei to determine if these eigenfunctions satisfy these pseudospin symmetry constraints.

PACS numbers: 24.10.Jv, 21.60.Cs, 24.80.+y, 21.10.-k

Keywords: Relativistic mean field theory; Symmetry; Dirac Hamiltonian; Pseudospin

I. INTRODUCTION

Pseudospin doublets were introduced more than thirty years ago into nuclear physics to accommodate an observed near degeneracy of certain normal parity shell model orbitals with non-relativistic quantum numbers ($n_r, \ell, j = \ell + 1/2$) and ($n_r - 1, \ell + 2, j = \ell + 3/2$) where n_r , ℓ , and j are the single-nucleon radial, orbital, and total angular momentum quantum numbers, respectively [1, 2]. The doublet structure is expressed in terms of a “pseudo” orbital angular momentum, which is an average of the orbital angular momentum of the two orbits in the doublet, $\tilde{\ell} = \ell + 1$, coupled to a “pseudo” spin, $\tilde{s} = 1/2$ with $j = \tilde{\ell} \pm \tilde{s}$. For example, the shell model orbitals ($n_r s_{1/2}, (n_r - 1) d_{3/2}$) will have $\tilde{\ell} = 1$, ($n_r p_{3/2}, (n_r - 1) f_{5/2}$) will have $\tilde{\ell} = 2$, for the two states in the doublet. Then the single-particle energy is approximately independent of the orientation of the pseudospin leading to an approximate pseudospin symmetry. These doublets persist for deformed nuclei as well [3]. The axially-symmetric deformed single-particle orbits with non-relativistic asymptotic quantum numbers $[N, n_3, \Lambda]\Omega = \Lambda + 1/2$ and $[N, n_3, \Lambda']\Omega' = \Lambda + 2|\Omega'| = \Lambda + 3/2$ are quasi-degenerate. Here N is the total harmonic oscillator quantum number, n_3 is the number of quanta for oscillations along the symmetry axis, taken to be in the z -direction, Λ and Ω are respectively the components of the orbital and total angular momentum projected along the symmetry axis [4]. In this case, the doublet structure is expressed in terms of a “pseudo” orbital angular momentum projection, $\tilde{\Lambda} = \Lambda + 1$, which is added to a “pseudo” spin projection, $\tilde{\mu} = \pm 1/2$ to yield the above mentioned doublet of states with $\Omega = \tilde{\Lambda} - 1/2$ and $\Omega' = \tilde{\Lambda} + 1/2$. This approximate pseudospin “symmetry” has been used to explain features of deformed nuclei, including superdeformation [5] and identical bands [6, 7, 8, 9] as well.

Although there have been attempts to understand the origin of this “symmetry” [10, 11], only recently has it been shown to arise from a relativistic symmetry of the Dirac Hamiltonian [12, 13] which we review in Section II. This relativistic symmetry implies conditions on the Dirac eigenfunctions [14] which we discuss in Sections II and III. These relationships have been studied extensively [14, 15, 16, 17, 18, 19] for spherical nuclei. For deformed nuclei, the relationships have been studied only in a limited way and primarily for the lower components of the Dirac eigenfunctions [20, 21, 22]. In this paper we shall test thoroughly these relationships between the upper and lower components of the two states in the doublet for realistic deformed relativistic eigenfunctions [23, 24].

*Electronic address: gino@t5.lanl.gov

†Electronic address: ami@vms.huji.ac.il

‡Electronic address: mengj@pku.edu.cn

§Electronic address: sgzhou@mpi-hd.mpg.de

II. THE DIRAC HAMILTONIAN AND PSEUDOSPIN SYMMETRY

The Dirac Hamiltonian, H , with an external scalar, $V_S(\vec{r})$, and vector, $V_V(\vec{r})$, potentials is given by:

$$H = \hat{\alpha} \cdot \mathbf{p} + \hat{\beta} (M + V_S(\vec{r})) + V_V(\vec{r}), \quad (1)$$

where $\hat{\alpha}, \hat{\beta}$ are the usual Dirac matrices, M is the nucleon mass, and we have set $\hbar = c = 1$. The Dirac Hamiltonian is invariant under a SU(2) algebra for two limits: $V_S(\vec{r}) = V_V(\vec{r}) + C_s$ and $V_S(\vec{r}) = -V_V(\vec{r}) + C_{ps}$ where C_s, C_{ps} are constants [25]. The former limit has application to the spectrum of mesons for which the spin-orbit splitting is small [26] and for the spectrum of an antinucleon in the mean-field of nucleons [27, 28]. The latter limit leads to pseudospin symmetry in nuclei [12]. This symmetry occurs independent of the shape of the nucleus: spherical, axial deformed, or triaxial.

A. Pseudospin Symmetry Generators

The generators for the pseudospin SU(2) algebra, \tilde{S}_i ($i = x, y, z$), which commute with the Dirac Hamiltonian, $[H_{ps}, \tilde{S}_i] = 0$, for the pseudospin symmetry limit $V_S(\vec{r}) = -V_V(\vec{r}) + C_{ps}$, are given by [13]

$$\tilde{S}_i = \begin{pmatrix} \tilde{s}_i & 0 \\ 0 & s_i \end{pmatrix} = \begin{pmatrix} U_p s_i U_p & 0 \\ 0 & s_i \end{pmatrix} \quad (2)$$

where $s_i = \sigma_i/2$ are the usual spin generators, σ_i the Pauli matrices, and $U_p = \frac{\boldsymbol{\sigma} \cdot \mathbf{p}}{p}$ is the momentum-helicity unitary operator introduced in [11]. Thus the operators \tilde{S}_i generate an SU(2) invariant symmetry of H_{ps} . Therefore, each eigenstate of the Dirac Hamiltonian has a partner with the same energy,

$$H_{ps} \Phi_{\tilde{k}, \tilde{\mu}}^{ps}(\vec{r}) = E_{\tilde{k}} \Phi_{\tilde{k}, \tilde{\mu}}^{ps}(\vec{r}) \quad (3)$$

where \tilde{k} are the other quantum numbers and $\tilde{\mu} = \pm \frac{1}{2}$ is the eigenvalue of \tilde{S}_z ,

$$\tilde{S}_z \Phi_{\tilde{k}, \tilde{\mu}}^{ps}(\vec{r}) = \tilde{\mu} \Phi_{\tilde{k}, \tilde{\mu}}^{ps}(\vec{r}). \quad (4)$$

The eigenstates in the doublet will be connected by the generators $\tilde{S}_{\pm} = \tilde{S}_x \pm i \tilde{S}_y$,

$$\tilde{S}_{\pm} \Phi_{\tilde{k}, \tilde{\mu}}^{ps}(\vec{r}) = \sqrt{\left(\frac{1}{2} \mp \tilde{\mu}\right) \left(\frac{3}{2} \pm \tilde{\mu}\right)} \Phi_{\tilde{k}, \tilde{\mu} \pm 1}^{ps}(\vec{r}). \quad (5)$$

The fact that Dirac eigenfunctions belong to the spinor representation of the pseudospin SU(2), as given in Eqs. (4)-(5), leads to the conditions on the corresponding Dirac amplitudes that are explored in this paper and developed in the next Subsection.

B. Dirac Eigenfunctions and Pseudospin Symmetry

An eigenstate $\Phi_{\tilde{k}, \tilde{\mu}}^{ps}(\vec{r})$ of the Dirac Hamiltonian H_{ps} , Eq. (3), is a four-dimensional vector,

$$\Phi_{\tilde{k}, \tilde{\mu}}^{ps}(\vec{r}) = \begin{pmatrix} g_{\tilde{k}, \tilde{\mu}}^+(\vec{r}) \\ g_{\tilde{k}, \tilde{\mu}}^-(\vec{r}) \\ i f_{\tilde{k}, \tilde{\mu}}^+(\vec{r}) \\ i f_{\tilde{k}, \tilde{\mu}}^-(\vec{r}) \end{pmatrix}, \quad (6)$$

where $g_{\tilde{k}, \tilde{\mu}}^{\pm}(\vec{r})$ are the “upper Dirac components” and $f_{\tilde{k}, \tilde{\mu}}^{\pm}(\vec{r})$ are the “lower Dirac components”. The superscript $+$ ($-$) indicates spin up (spin down).

The connections between the Dirac eigenstates of the doublet ($\tilde{\mu} = \pm \frac{1}{2}$) resulting from Eqs. (4)-(5) lead to relationships between the Dirac amplitudes in Eq. (6) [14],

$$f_{\tilde{k}, -\frac{1}{2}}^+(\vec{r}) = f_{\tilde{k}, \frac{1}{2}}^-(\vec{r}) = 0 , \quad (7a)$$

$$f_{\tilde{k}, \frac{1}{2}}^+(\vec{r}) = f_{\tilde{k}, -\frac{1}{2}}^-(\vec{r}) \equiv f_{\tilde{k}}(\vec{r}) , \quad (7b)$$

$$g_{\tilde{k}, \frac{1}{2}}^+(\vec{r}) = -g_{\tilde{k}, -\frac{1}{2}}^-(\vec{r}) \equiv g_{\tilde{k}}(\vec{r}) , \quad (7c)$$

and to first order differential equations,

$$\left(\frac{\partial}{\partial x} - i \frac{\partial}{\partial y} \right) g_{\tilde{k}, \frac{1}{2}}^-(\vec{r}) = \left(\frac{\partial}{\partial x} + i \frac{\partial}{\partial y} \right) g_{\tilde{k}, -\frac{1}{2}}^+(\vec{r}) , \quad (8a)$$

$$\frac{\partial}{\partial z} g_{\tilde{k}, \mp \frac{1}{2}}^\pm(\vec{r}) = \pm \left(\frac{\partial}{\partial x} \mp i \frac{\partial}{\partial y} \right) g_{\tilde{k}, \pm \frac{1}{2}}^\pm(\vec{r}) . \quad (8b)$$

Thus pseudospin symmetry reduces the eight amplitudes for the two states in the doublet to four amplitudes. In the next Section we shall discuss these relations in Eqs. (7)-(8) for axially deformed nuclei.

III. PSEUDOSPIN SYMMETRY FOR AXIALLY DEFORMED NUCLEI

If the potentials are axially symmetric, that is, independent of the azimuthal angle ϕ , $V_{S,V}(\vec{r}) = V_{S,V}(\rho, z)$, $\rho = \sqrt{x^2 + y^2}$, then the Dirac Hamiltonian has an additional U(1) symmetry in the pseudospin limit. The conserved $U(1)$ generator is given by [13]

$$\tilde{L}_z = \begin{pmatrix} \tilde{\ell}_z & 0 \\ 0 & \ell_z \end{pmatrix} . \quad (9)$$

where $\tilde{\ell}_z = U_p \ell_z U_p$ and $\ell_z = (\mathbf{r} \times \mathbf{p})_z$. In this case, the Dirac eigenstates of H_{ps} are simultaneous eigenstates of \tilde{L}_z , with eigenvalue $\tilde{\Lambda}$, and of the total angular momentum generator $J_z = \tilde{S}_z + \tilde{L}_z$, with eigenvalues $\Omega = \tilde{\Lambda} + \tilde{\mu} = \tilde{\Lambda} \pm \frac{1}{2}$

$$\begin{aligned} \tilde{L}_z \Phi_{\tilde{\eta}, \tilde{\Lambda}, \tilde{\mu}, \Omega}^{ps}(\vec{r}) &= \tilde{\Lambda} \Phi_{\tilde{\eta}, \tilde{\Lambda}, \tilde{\mu}, \Omega}^{ps}(\vec{r}) , \\ J_z \Phi_{\tilde{\eta}, \tilde{\Lambda}, \tilde{\mu}, \Omega}^{ps}(\vec{r}) &= \Omega \Phi_{\tilde{\eta}, \tilde{\Lambda}, \tilde{\mu}, \Omega}^{ps}(\vec{r}) . \end{aligned} \quad (10)$$

Here $\tilde{\eta}$ denotes additional quantum numbers that may be needed to specify the states uniquely.

The conventional method of labeling the eigenstates of axially deformed single-particle states in nuclei is to use the asymptotic quantum numbers $(N, n_3, \Lambda, \Omega)$, mentioned in the Introduction, that emerge in the limit of a non-relativistic axially-symmetric deformed harmonic oscillator with spin symmetry. For the relativistic axially-deformed harmonic oscillator with spin symmetry [29] the eigenfunctions can also be labeled by these quantum numbers. However, only the spatial amplitudes of the upper components of the doublet will necessarily have the nodes suggested by these quantum numbers, whereas the spatial amplitudes of the lower components may have different nodal structure. For spherically symmetric potentials a general theorem relates the nodal structure of the upper and lower Dirac amplitudes, and has been used to explain the non-relativistic radial quantum numbers characterizing pseudospin doublets in spherical nuclei [30]. A corresponding theorem for axially-deformed potentials in the pseudospin and spin limits of the Dirac Hamiltonian appears to hold under certain conditions which the relativistic harmonic oscillator satisfies, but which do not generally apply for realistic axially-symmetric potentials [31]. For the latter, only the quantum numbers $\tilde{\Lambda}$ and Ω in Eq. (10) are conserved in the pseudospin limit. The fact that the axial-symmetry of the potentials determines the ϕ -dependence of the Dirac wave functions, leads to the following form for the relativistic pseudospin doublet eigenstates [14]

$$\Phi_{\tilde{\eta}, \tilde{\Lambda}, -\frac{1}{2}, \Omega=\tilde{\Lambda}-\frac{1}{2}}^{ps}(\vec{r}) = \begin{pmatrix} g_{\tilde{\eta}, \tilde{\Lambda}, -\frac{1}{2}}^+(\rho, z) e^{i(\tilde{\Lambda}-1)\phi} \\ -g_{\tilde{\eta}, \tilde{\Lambda}}(\rho, z) e^{i\tilde{\Lambda}\phi} \\ 0 \\ if_{\tilde{\eta}, \tilde{\Lambda}}(\rho, z) e^{i\tilde{\Lambda}\phi} \end{pmatrix} , \quad \Omega = \tilde{\Lambda} - \frac{1}{2} , \quad (11a)$$

$$\Phi_{\tilde{\eta}, \tilde{\Lambda}, \frac{1}{2}, \Omega' = \tilde{\Lambda} + \frac{1}{2}}^{ps}(\vec{r}) = \begin{pmatrix} g_{\tilde{\eta}, \tilde{\Lambda}}(\rho, z) e^{i\tilde{\Lambda}\phi} \\ g_{\tilde{\eta}, \tilde{\Lambda}, \frac{1}{2}}^-(\rho, z) e^{i(\tilde{\Lambda}+1)\phi} \\ i f_{\tilde{\eta}, \tilde{\Lambda}}(\rho, z) e^{i\tilde{\Lambda}\phi} \\ 0 \end{pmatrix}, \quad \Omega' = \tilde{\Lambda} + \frac{1}{2}. \quad (11b)$$

The two states in the doublet have the same pseudo-orbital angular momentum projection along the symmetry axis, $\tilde{\Lambda}$, but different total angular momentum projections $\Omega = \tilde{\Lambda} - \frac{1}{2}$ and $\Omega' = \tilde{\Lambda} + \frac{1}{2}$. As seen from Eqs. (11a) and (11b), the pseudospin projection, $\tilde{\mu} = \pm \frac{1}{2}$, and $\tilde{\Lambda}$ are respectively the ordinary spin projection and ordinary orbital angular momentum projection of the non-vanishing lower component $f_{\tilde{\eta}, \tilde{\Lambda}}(\rho, z)$. The corresponding dominant upper components $g_{\tilde{\eta}, \Lambda, -\frac{1}{2}}^+(\rho, z)$ and $g_{\tilde{\eta}, \Lambda, \frac{1}{2}}^-(\rho, z)$ have orbital angular momentum projections $\Lambda = \tilde{\Lambda} - 1$ and $\Lambda' = \tilde{\Lambda} + 1$ respectively, hence $\Lambda' = \Lambda + 2$. Accordingly, $\Omega = \Lambda + 1/2$ and $\Omega' = \Lambda' - 1/2 = \Lambda + 3/2$. These assignments agree with the non-relativistic pseudospin quantum numbers discussed in the Introduction. The generic label $\tilde{\eta}$ in $\Phi_{\tilde{\eta}, \tilde{\Lambda}, \tilde{\mu}, \Omega}^{ps}(\vec{r})$ replaces the harmonic oscillator labels N and n_3 , which are not conserved for realistic axially-deformed potentials in nuclei.

In obtaining the expressions in Eq. (11) we have used the relations in Eq. (7), which for axially-deformed potentials read [14]

$$f_{\tilde{\eta}, \tilde{\Lambda}, -\frac{1}{2}}^+(\rho, z) = f_{\tilde{\eta}, \tilde{\Lambda}, \frac{1}{2}}^-(\rho, z) = 0, \quad (12a)$$

$$f_{\tilde{\eta}, \tilde{\Lambda}, \frac{1}{2}}^+(\rho, z) = f_{\tilde{\eta}, \tilde{\Lambda}, -\frac{1}{2}}^-(\rho, z) \equiv f_{\tilde{\eta}, \tilde{\Lambda}}(\rho, z), \quad (12b)$$

$$g_{\tilde{\eta}, \tilde{\Lambda}, \frac{1}{2}}^+(\rho, z) = -g_{\tilde{\eta}, \tilde{\Lambda}, -\frac{1}{2}}^-(\rho, z) \equiv g_{\tilde{\eta}, \tilde{\Lambda}}(\rho, z), \quad (12c)$$

and the differential relations (8) become

$$\left(\frac{\partial}{\partial \rho} + \frac{\tilde{\Lambda} + 1}{\rho} \right) g_{\tilde{\eta}, \tilde{\Lambda}, \frac{1}{2}}^-(\rho, z) = \left(\frac{\partial}{\partial \rho} - \frac{\tilde{\Lambda} - 1}{\rho} \right) g_{\tilde{\eta}, \tilde{\Lambda}, -\frac{1}{2}}^+(\rho, z), \quad (13a)$$

$$\frac{\partial}{\partial z} g_{\tilde{\eta}, \tilde{\Lambda}, \mp \frac{1}{2}}^\pm(\rho, z) = \pm \left(\frac{\partial}{\partial \rho} \pm \frac{\tilde{\Lambda}}{\rho} \right) g_{\tilde{\eta}, \tilde{\Lambda}, \pm \frac{1}{2}}^\pm(\rho, z). \quad (13b)$$

We shall now test to see if the pseudospin symmetry conditions in Eqs. (12)-(13) are valid for realistic relativistic mean field eigenfunctions in deformed nuclei.

IV. COMPARISON WITH REALISTIC RELATIVISTIC EIGENFUNCTIONS

The single-particle energies and wave functions for ^{168}Er are calculated by the relativistic Hartree theory with the parameter set NL3 in a Woods-Saxon basis [23, 24]. This method has been developed from relativistic theory in coordinate space [32, 33, 34] and has the advantage that it easily generalizes to include both deformation and pairing correction self-consistently. The pairing correlation is treated with the BCS approximation. These calculations lead to a theoretical average binding energy $B/A = 8.107$ MeV, a quadrupole deformation $\beta = 0.3497$ and a root mean square radius $R = 5.376$ fm, which reproduce the data well. For these realistic eigenfunctions the harmonic oscillator quantum numbers are not conserved, but the orbitals are labeled by the quantum numbers of the main spherical basis state in the expansion of the dominant upper component in the Dirac eigenfunctions.

In Figure 1, the calculated single-neutron energies, $\varepsilon = E - M$, for the pseudospin doublets in ^{168}Er are presented. From left to right, the panels correspond to the pseudo orbital angular momentum projection $\tilde{\Lambda} = 1, 2, 3$ and 4 , respectively. The energy splitting between members of pseudospin doublets decreases as the single-particle binding energy, $-\varepsilon$, decreases. For pseudospin doublets with binding energy larger than 5 MeV, the spin-up (pseudospin down) state is higher than the spin-down (pseudospin up) one. On the other hand, for the bound doublets with binding energy less than 5 MeV, the opposite is observed.

Four pairs of neutron pseudospin partners are chosen to illustrate the relations given above. (i) The states $[402]\frac{5}{2}^-$ and $[404]\frac{7}{2}^-$ ($\tilde{\Lambda} = 3$), which have a large energy splitting (about 2 MeV). The single-particle energies are respectively $\varepsilon_{[402]\frac{5}{2}^-} = -12.083$ and $\varepsilon_{[404]\frac{7}{2}^-} = -14.160$ MeV. (ii) The states $[400]\frac{1}{2}^+$ and $[402]\frac{3}{2}^+$ ($\tilde{\Lambda} = 1$), which have a small energy

splitting (about 0.4 MeV). The single-particle energies are respectively $\varepsilon_{[400]\frac{1}{2}} = -10.2073$ and $\varepsilon_{[404]\frac{7}{2}} = -10.603$ MeV. (iii) The states $[501]\frac{3}{2}$ and $[503]\frac{5}{2}$ ($\tilde{\Lambda} = 2$), which have a small energy splitting (less than 0.4 MeV). The single-particle energies are respectively $\varepsilon_{[501]\frac{3}{2}} = -1.349$ and $\varepsilon_{[503]\frac{5}{2}} = -0.9603$ MeV. (iv) The states $[510]\frac{1}{2}$ and $[512]\frac{3}{2}$ ($\tilde{\Lambda} = 1$), which have a tiny energy splitting (less than 0.01 MeV). The single-particle energies are respectively $\varepsilon_{[510]\frac{1}{2}} = -3.8436$ and $\varepsilon_{[512]\frac{3}{2}} = -3.8378$ MeV.

Plots for the above four pairs of neutron pseudospin partners are shown in Figures 2, 4, 6, 8, as a function of z for three segments: $\rho = 1, 3, 5$ fm, and in Figures 3, 5, 7, 9, as a function of ρ for three segments: $z = 1, 3, 5$ fm. In each segment the top row displays the relationships between lower component amplitudes given in Eqs. (12a)-(12b), and the relationship between upper component amplitudes given in Eq. (12c). The bottom row displays the differential relationships between upper component amplitudes given in Eq. (13).

From these figures, we can draw a number of conclusions. First, while the amplitudes $f_{\tilde{\eta}, \tilde{\Lambda}, -\frac{1}{2}}^+(\rho, z)$, $f_{\tilde{\eta}, \tilde{\Lambda}, \frac{1}{2}}^-(\rho, z)$ are not zero as predicted by Eq. (12a), they are much smaller than $f_{\tilde{\eta}, \tilde{\Lambda}, -\frac{1}{2}}^-(\rho, z)$, $f_{\tilde{\eta}, \tilde{\Lambda}, \frac{1}{2}}^+(\rho, z)$. Furthermore, $f_{\tilde{\eta}, \tilde{\Lambda}, \frac{1}{2}}^+(\rho, z)$ and $f_{\tilde{\eta}, \tilde{\Lambda}, -\frac{1}{2}}^-(\rho, z)$ have similar shapes as predicted by Eq. (12b). In Figures 2-3 for the $[402]5/2$, $[404]7/2$, $\tilde{\Lambda} = 3$ doublet there is some discrepancy in the shapes but the shapes become more equal as both the pseudo-orbital angular momentum projection $\tilde{\Lambda}$ decreases (see Figures 4-5 for the $[400]1/2$, $[402]3/2$, $\tilde{\Lambda} = 1$ doublet) and the binding energy decreases (see Figures 6-7 for the $[501]3/2$, $[503]5/2$, $\tilde{\Lambda} = 2$ doublet).

The amplitude $-g_{\tilde{\eta}, \tilde{\Lambda}, -\frac{1}{2}}^-(\rho, z)$ has the same shape as the amplitude $g_{\tilde{\eta}, \tilde{\Lambda}, \frac{1}{2}}^+(\rho, z)$, in line with the prediction of Eq. (12c), but they differ in magnitude. Again the discrepancy decreases as the pseudo-orbital angular momentum projection $\tilde{\Lambda}$ decreases (compare Figures 2-3 for the $[402]5/2$, $[404]7/2$, $\tilde{\Lambda} = 3$ doublet with Figures 8-9 for the $[510]1/2$, $[512]3/2$, $\tilde{\Lambda} = 1$ doublet) and the binding energy decreases (compare Figures 2-3 for the $[402]5/2$, $[404]7/2$, $\tilde{\Lambda} = 3$ doublet with Figure 6-7 for the $[501]3/2$, $[503]5/2$, $\tilde{\Lambda} = 2$ doublet or Figures 8-9 for the $[510]1/2$, $[512]3/2$, $\tilde{\Lambda} = 1$ doublet). These amplitudes are much smaller than the other upper amplitudes, $g_{\tilde{\eta}, \tilde{\Lambda}, \pm\frac{1}{2}}^\pm(\rho, z)$.

The differential relation in Eq. (13a) between the dominant upper components, $g_{\tilde{\eta}, \tilde{\Lambda}, \frac{1}{2}}^-(\rho, z)$ and $g_{\tilde{\eta}, \tilde{\Lambda}, -\frac{1}{2}}^+(\rho, z)$, is well obeyed in all cases. The differential relations in Eq. (13b) relate the dominant upper components, $g_{\tilde{\eta}, \tilde{\Lambda}, \pm\frac{1}{2}}^\pm(\rho, z)$ to the small upper components $g_{\tilde{\eta}, \tilde{\Lambda}, \pm\frac{1}{2}}^\pm(\rho, z)$. The shapes of the left-hand-side and of the right-hand-side of Eq. (13b) are the same, but the corresponding amplitudes are quite different. Therefore, the differential relations in Eq. (13b) are less satisfied. These differences might partly originate from the differences in the magnitudes of the small upper components in Eq. (12c).

V. SUMMARY

We have reviewed the conditions that pseudospin symmetry places on the Dirac eigenfunctions. We have shown that the conditions on the lower amplitudes, Eqs. (12a)-(12b), are approximately satisfied for axially deformed nuclei. The differential relation between the dominant upper component amplitudes, Eq. (13a), is also approximately satisfied. However, both the relation between the amplitudes of the small upper components, Eq. (12c), and the differential equations, Eq. (13b), that relate the dominant upper components with the small upper components are not well satisfied. The pseudospin symmetry improves as the binding energy and pseudo-orbital angular momentum projection decrease, which is consistent with previous tests of pseudospin symmetry in spherical nuclei.

This research was supported in part by the United States Department of Energy under contract W-7405-ENG-36, in part by a grant from the US-Israel Binational Science Foundation and in part by the Major State Basic Research Development Program Under Contract Number G2000077407 and the National Natural Science Foundation of China under Grant No. 10025522, 10221003, 10047001 and 19935030.

- [1] A. Arima, M. Harvey and K. Shimizu, Phys. Lett. B **30**, 517 (1969).
- [2] K.T. Hecht and A. Adler, Nucl. Phys. A **137**, 129 (1969).
- [3] A. Bohr, I. Hamamoto and B. R. Mottelson, Phys. Scr. **26**, 267 (1982).
- [4] A. Bohr and B. R. Mottelson, *Nuclear Structure*, Vol. II (W. A. Benjamin, Reading, Ma., 1975).
- [5] J. Dudek, W. Nazarewicz, Z. Szymanski and G. A. Leander, Phys. Rev. Lett. **59**, 1405 (1987).
- [6] W. Nazarewicz, P. J. Twin, P. Fallon and J.D. Garrett, Phys. Rev. Lett. **64**, 1654 (1990).
- [7] F. S. Stephens *et al*, Phys. Rev. Lett. **65**, 301 (1990); F. S. Stephens *et al*, Phys. Rev. C **57**, R1565 (1998).

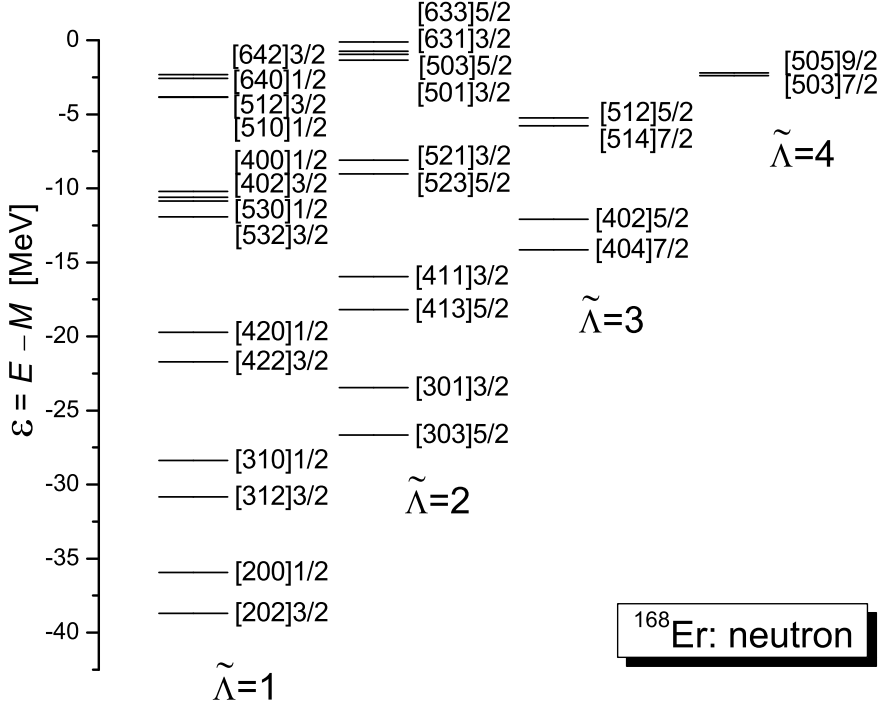


FIG. 1: The neutron spectra in MeV for the pseudospin doublets in ^{168}Er .

- [8] J. Y. Zeng, J. Meng, C. S. Wu, E. G. Zhao, Z. Xing and X. Q. Chen, Phys. Rev. C **44**, R1745 (1991).
- [9] A.M. Bruce *et. al.*, Phys. Rev. C **56**, 1438 (1997).
- [10] C. Bahri, J. P. Draayer, and S. A. Moszkowski, Phys. Rev. Lett. **68**, 2133 (1992).
- [11] A. L. Blokhin, C. Bahri, and J. P. Draayer, Phys. Rev. Lett. **74**, 4149 (1995).
- [12] J.N. Ginocchio, Phys. Rev. Lett. **78**, 436 (1997).
- [13] J. N. Ginocchio and A. Leviatan, Phys. Lett. B **425**, 1 (1998).
- [14] J.N. Ginocchio, Phys. Rev. C **66**, 064312 (2002).
- [15] J. N. Ginocchio and D. G. Madland, Phys. Rev. C **57**, 1167 (1998).
- [16] G.A. Lalazissis, Y.K. Gambhir, J.P. Maharana, C.S. Warke and P. Ring, Phys. Rev. C **58**, R45 (1998).
- [17] J. Meng, K. Sugawara-Tanabe, S. Yamaji, P. Ring and A. Arima, Phys. Rev. C **58**, R628 (1998); J. Meng, K. Sugawara-Tanabe, S. Yamaji and A. Arima, Phys. Rev. C **59**, 154 (1999).
- [18] J.N. Ginocchio and A. Leviatan, Phys. Rev. Lett. **87**, 072502 (2001).
- [19] P.J. Borycki, J. Ginocchio, W. Nazarewicz, and M. Stoitsov, Phys. Rev. C **68**, 014304 (2003).
- [20] K. Sugawara-Tanabe and A. Arima, Phys. Rev. C **58**, R3065 (1998).
- [21] K. Sugawara-Tanabe, S. Yamaji, and A. Arima, Phys. Rev. C **62**, 054307 (2000).
- [22] K. Sugawara-Tanabe, S. Yamaji, and A. Arima, Phys. Rev. C **65**, 054313 (2002).
- [23] S. G. Zhou, J. Meng, S. Yamaji and S. C. Yang, Chinese Phys. Lett. **17**, 717 (2000).
- [24] S. G. Zhou, J. Meng, P. Ring, Phys. Rev. C **68**, 034323 (2003).
- [25] J. S. Bell and H. Ruegg, Nucl. Phys. B **98**, 151 (1975).
- [26] P.R. Page, T. Goldman, and J. N. Ginocchio, Phys. Rev. Lett. **86**, 204 (2001).
- [27] J. N. Ginocchio, Phys. Rep. **315**, 231 (1999).
- [28] S. G. Zhou, J. Meng, and P. Ring, to be published in Phys. Rev. Lett. (2003); nucl-th/0304067.
- [29] J.N. Ginocchio, to be published in Phys. Rev. C, (2003).
- [30] A. Leviatan and J.N. Ginocchio, Physics Letters B **518**, 214 (2001).
- [31] A. Leviatan, J.N. Ginocchio, and T. Bürvenich, work in progress.
- [32] J. Meng and P. Ring, Phys. Rev. Lett. **77**, 3963 (1996).
- [33] J. Meng, Nucl. Phys. A **635**, 3 (1998).
- [34] J. Meng and P. Ring, Phys. Rev. Lett. **80**, 460 (1998).

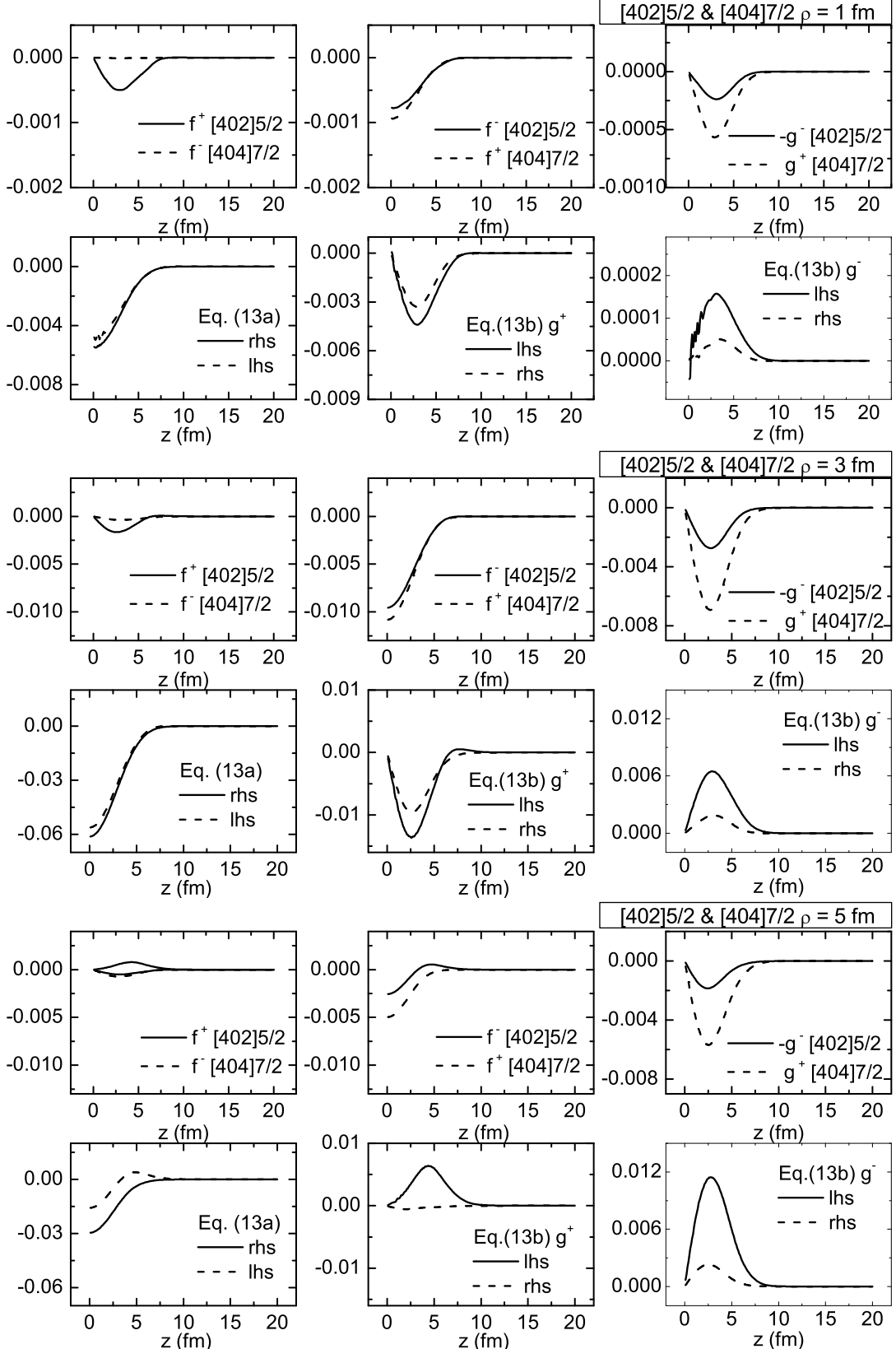


FIG. 2: Wave functions in $(\text{Fermi})^{-3/2}$ as a function of z and $\rho = 1, 3, 5$ fm for the neutron pseudospin doublet $[402]5/2$ and $[404]7/2$ ($\tilde{\Lambda} = 3$) in ^{168}Er . In each segment, the top row shows (from left to right) the relations in (i) Eq. (12a), involving $f_{\eta,\tilde{\Lambda},-1/2}^+$ and $f_{\eta,\tilde{\Lambda},1/2}^-$, (ii) Eq. (12b), involving $f_{\eta,\tilde{\Lambda},-1/2}^-$ and $f_{\eta,\tilde{\Lambda},1/2}^+$, (iii) Eq. (12c), involving $g_{\eta,\tilde{\Lambda},1/2}^+$ and $-g_{\eta,\tilde{\Lambda},-1/2}^-$. The bottom row shows (from left to right) the lhs and rhs of (i) Eq. (13a), involving $g_{\eta,\tilde{\Lambda},\frac{1}{2}}^-$ and $g_{\eta,\tilde{\Lambda},-\frac{1}{2}}^+$, (ii) Eq. (13b), involving $g_{\eta,\tilde{\Lambda},-\frac{1}{2}}^+$ and $g_{\eta,\tilde{\Lambda},\frac{1}{2}}^-$, (iii) Eq. (13b), involving $g_{\eta,\tilde{\Lambda},+\frac{1}{2}}^-$ and $g_{\eta,\tilde{\Lambda},-\frac{1}{2}}^+$.

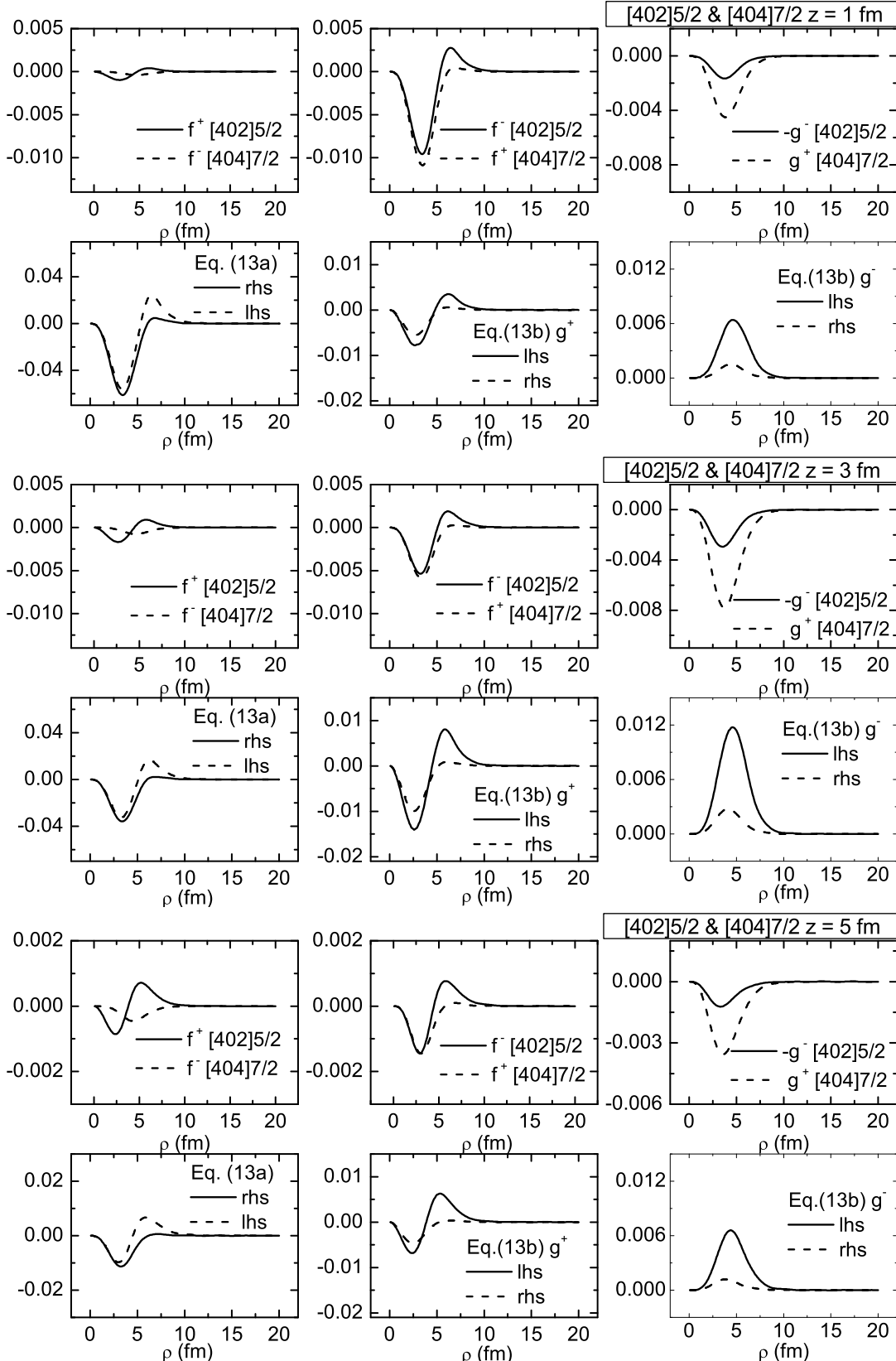


FIG. 3: Wave functions in $(\text{Fermi})^{-3/2}$ as a function of ρ and $z = 1, 3, 5$ fm for the neutron pseudospin doublet $[402]5/2$ and $[404]7/2$ ($\tilde{\Lambda} = 3$) in ^{168}Er . The content of the graphs in each segment as in Fig. 2.

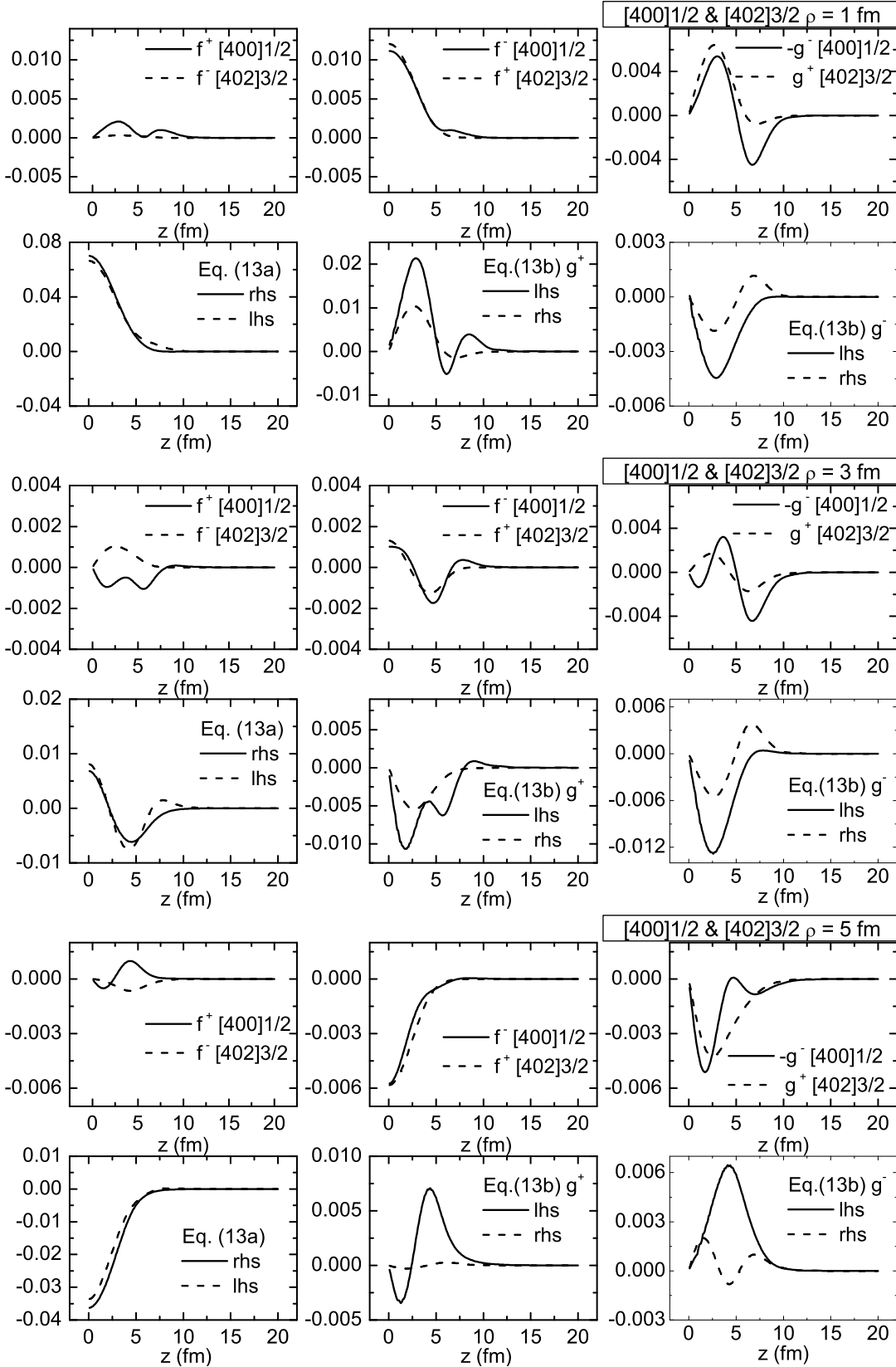


FIG. 4: As in Fig. 2 but for the neutron pseudospin doublet $[400]1/2$ and $[402]3/2$ ($\tilde{\Lambda} = 1$) in ^{168}Er .

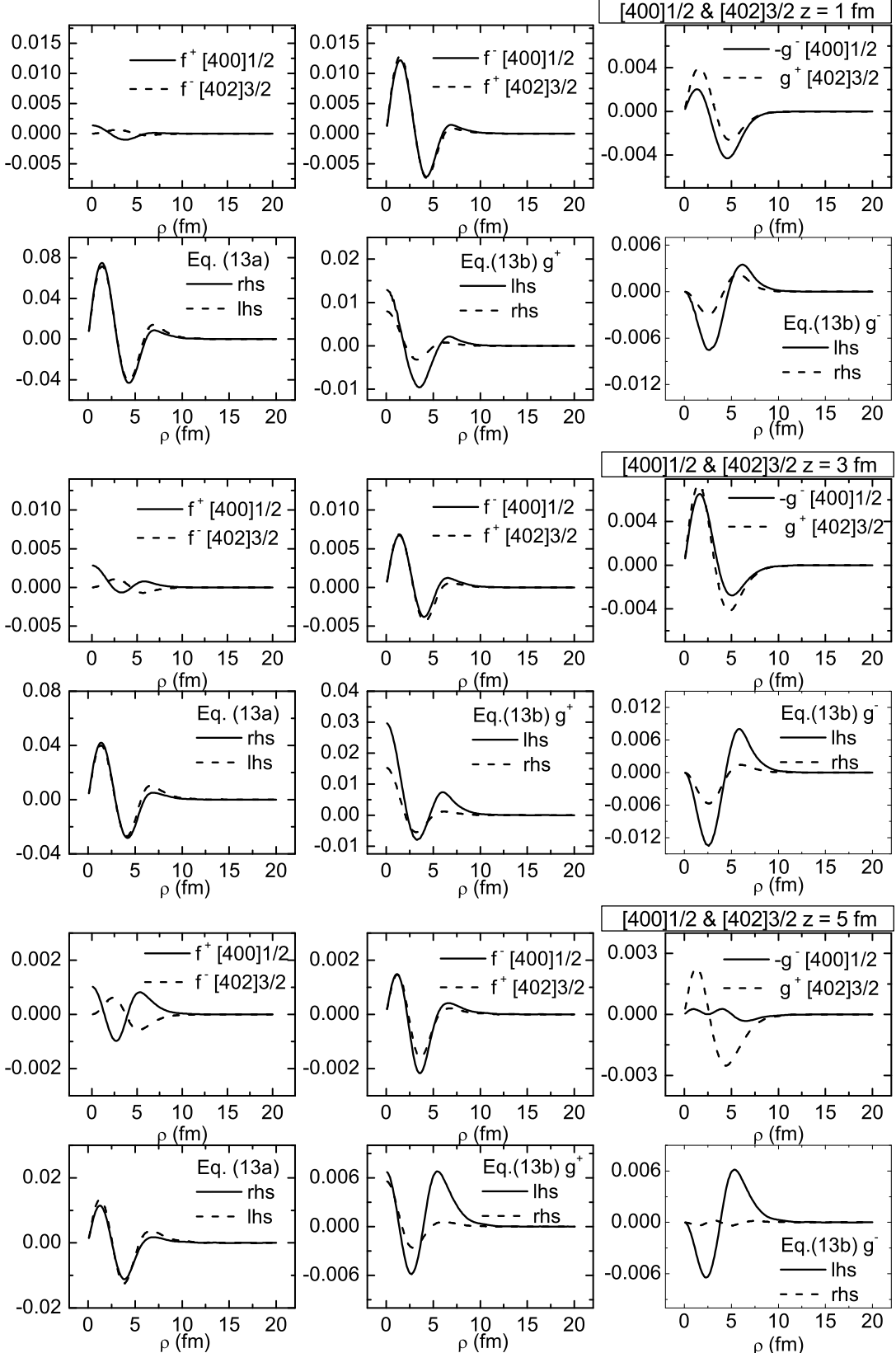


FIG. 5: As in Fig. 3 but for the neutron pseudospin doublet $[400]1/2$ and $[402]3/2$ ($\tilde{\Lambda} = 1$) in ^{168}Er .

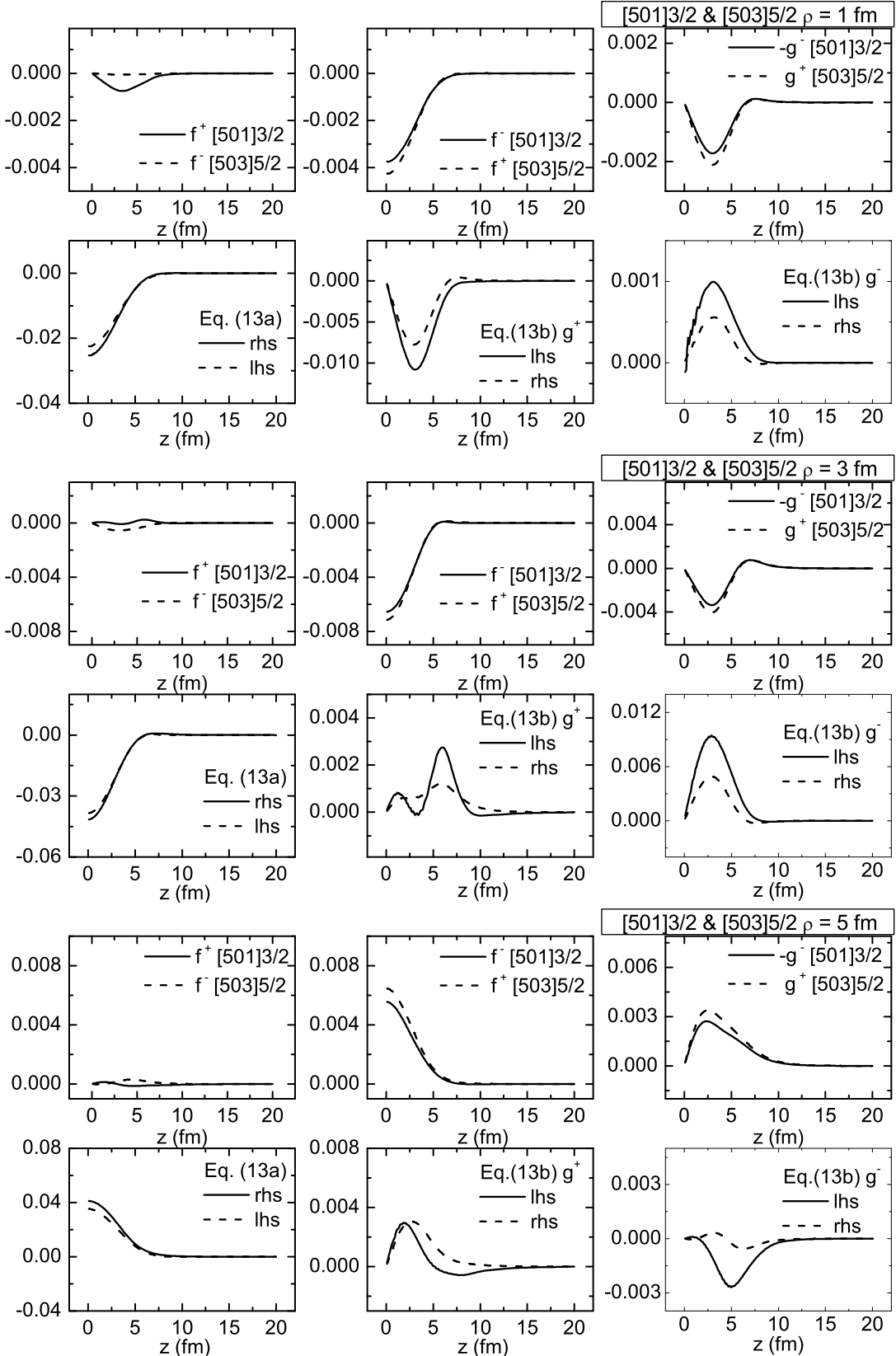


FIG. 6: As in Fig. 2 but for the neutron pseudospin doublet [501]3/2 and [503]5/2 ($\tilde{\Lambda} = 2$) in ^{168}Er .

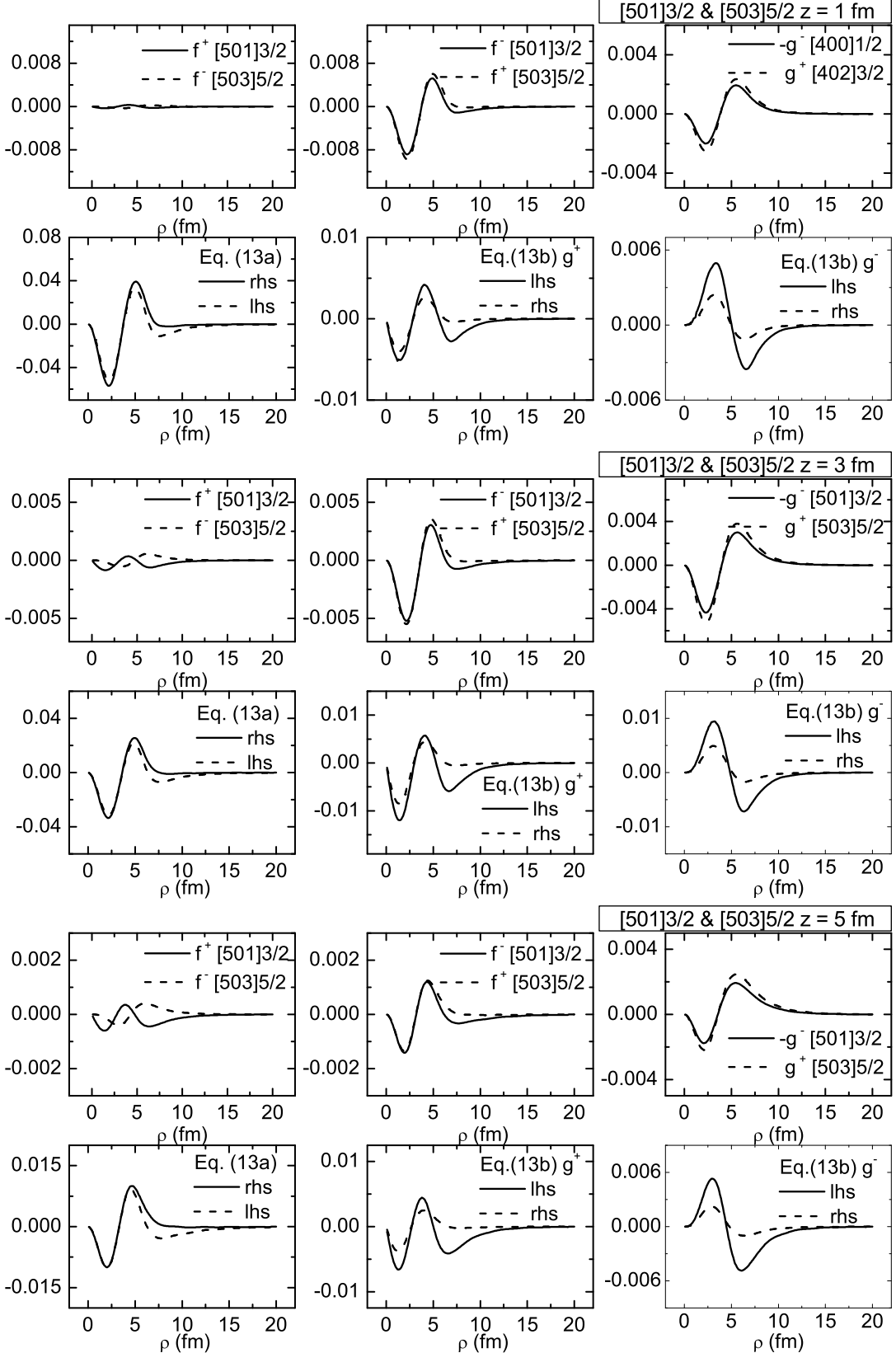


FIG. 7: As in Fig. 3 but for the neutron pseudospin doublet $[501]3/2$ and $[503]5/2$ ($\tilde{\Lambda} = 2$) in ^{168}Er .

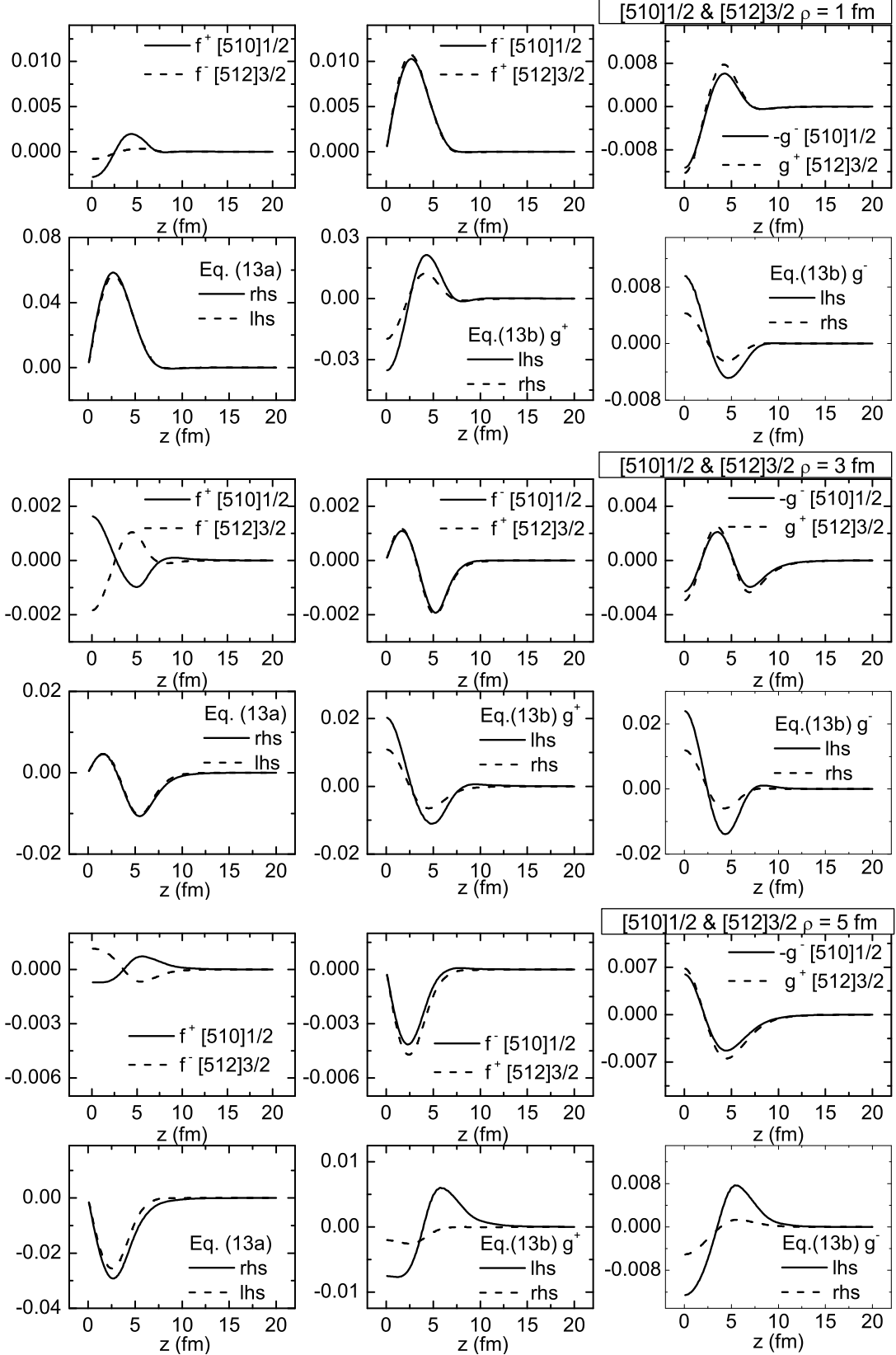


FIG. 8: As in Fig. 2 but for the neutron pseudospin doublet $[510]1/2$ and $[512]3/2$ ($\tilde{\Lambda} = 1$) in ^{168}Er .

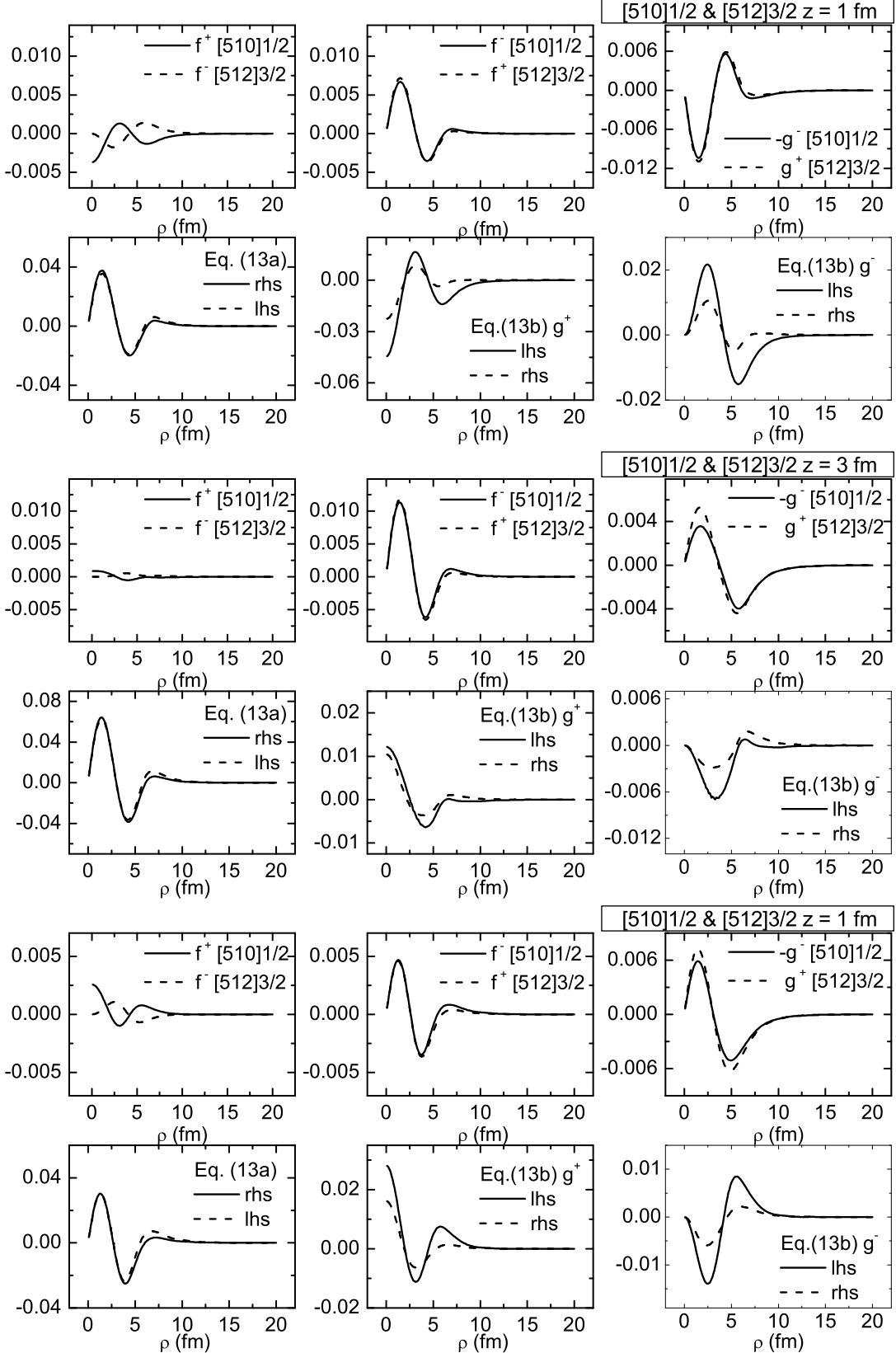


FIG. 9: As in Fig. 3 but for the neutron pseudospin doublet $[510]1/2$ and $[512]3/2$ ($\tilde{\Lambda} = 1$) in ^{168}Er .